# LTA/poly(1-trimethylsilyl-1-propyne) mixed-matrix membranes for high-temperature $CO_2/N_2$ separation

Ana Fernández-Barquín[1], Clara Casado-Coterillo[1,*], Miguel Palomino[2], Susana Valencia[2], Angel Irabien[1]

[1] *Universidad de Cantabria, Department of Chemical and Biomolecular Engineering, Av. Los Castros s/n, 39005 Santander, Spain*

[2] *UPV-CSIC, Instituto de Tecnología Química, Av. Los Naranjos s/n, 46022 Valencia, Spain.*

***Correspondence:** C. Casado-Coterillo (casadoc@unican.es), Universidad de Cantabria, Avda. Los Castros s/n, 39005 Santander, Spain.

**Abstract:** Mixed-matrix membranes (MMMs) comprised of poly(1-trimethylsilyl-1-propyne) (PTMSP) as continuous matrix and small pore LTA-framework zeolites with Si/Al from 1 (commercial zeolite A) to ∞ (ITQ-29) as dispersed phase, were prepared by solution casting at loadings in the range 5-20 wt. %. The thermal stability of the MMMs is as high as that of glassy PTMSP polymer, whose high permeability is maintained even upon increasing temperature. The effect of Si/Al ratio in zeolite fillers on the membrane performance is observed by the increasing $CO_2/N_2$ permselectivity of low Si/Al ratio zeolite A-based membranes, in comparison with pure silica ITQ-29. The $CO_2$ permeability of both membranes decreases with temperature, but in the case of zeolite A-PTMSP MMMs, the selectivity increases more due to higher decrease of $N_2$ permeability. This resulted in surpassing the Robeson's upper bound and expecting a good performance of these new hybrid membrane materials in $CO_2$ separation at higher temperature. The performance of LTA-type zeolite-PTMSP MMMs has been adjusted to the modified

Maxwell model by estimating the chain immobilization factor and the interphase thickness as a function of temperature, Si/Al and zeolite loading.

**Keywords:** Gas separation; Mixed-matrix membranes; Poly (1-trimethylsilyl-1-propyne); Thermal stability; LTA

## 1. Introduction

Carbon dioxide emissions from fossil fuel combustion are a major contributor to climate change. One step toward reducing $CO_2$ emissions is to capture the $CO_2$ generated during combustion and store it in a suitable place. This process of carbon capture and storage (CCS) has the potential to reduce future world emissions from energy by 20% [1] and carbon dioxide valorization is under development [2]. Post-combustion carbon capture appears to be the most amenable strategy to integration with existing coal-fired power plants. The key competing technologies for post-combustion carbon capture are absorption, adsorption and membrane gas separation [3]. Membrane technology is a simple and energy conservative separation method that has been much researched as an alternative to conventional processes.

Generally, thermal stability, durability, mechanical integrity at the operating conditions, productivity and separation efficiency are criteria for selecting membrane materials. Membrane materials stable in the presence of water vapor at temperatures up to 200°C would be excellent candidates for post-combustion processes, but their integration in high-temperature separation processes in more efficient power generation systems is still a challenging task [4, 5].

Inorganic membranes, such as zeolite membranes, have been studied during last decades due to zeolite capacity to discriminate between small molecules, as well high

thermal and chemical stability. However, their application at industrial level as membranes is strongly limited due to the manufacturing difficulties, reproducibility and cost [6] and most researchers have been focused on the basic characteristic of the novel materials and little is known about the applicability of the materials in processes at larger scale [7].

Polymers are the most advanced membrane materials on $CO_2$ separation processes. Although there are several commercial polymeric membranes, these have not been so far an alternative for $CO_2$ capture in large-scale power production. Two important reasons for this are insufficient performance in terms of selectivity and flux, where polymeric membranes usually show a trade-off on their permeability and selectivity for a specific gas-pair mixture separation [8], and secondly, the lack of high-temperature stability because of their restricted mechanical, chemical and thermal stability. Glassy polymer membranes show better thermal stability and mechanical properties, but they usually provide lower permeabilities than rubbery membranes [9].

Poly (1-trimethylsilyl-1-propyne) (PTMSP) has attracted much interest in the last 20 years because it has the highest known permeability of any polymer to gases and vapors despite its glassy nature. This is attributed to the presence of alternating double bonds in the backbone and a bulky trimethylsilyl [$Si(CH_3)_3$] side group [10]. This permeability is probably related to its extremely large free volume (0.29) and a very low density (0.75 g $cm^{-3}$), relative to that of other polymers [11]. The stiff chain, glassy structure accounts for the low chain mobility with glass transition temperature greater than 250ºC, which makes it a promising material for high-temperature membrane separations.

However, the high permeability of PTMSP is coupled with low ideal selectivity (the ratio of the single gas permeabilities of two permeants), and decreases rather

dramatically with time due to physical or chemical aging leading to relaxation of the enormous levels of excess free volume or due to oxidation of the double bonds in the chain backbone [12]. Many efforts have been directed to improve this for obtaining robust and durable membranes: crosslinking [13], substitution of functional groups [11], blending [14] and mixed matrix membranes [15].

Mixed-matrix membranes (MMMs) are emerging to face the challenges in membrane technology. MMMs combine the molecular sieving effect and catalytic properties of inorganic fillers and the processability of polymers to obtain a new material with improved mechanical and functional properties [16]. Material selection for both matrix and sieve phases is a key aspect in the development of mixed matrix membranes. Polymer matrix selection determines minimum membrane performance, and the addition of properly selected molecular sieves can only improve membrane selectivity in the absence of defects mostly due to inadequate adhesion between polymers and inorganic particles [17]. Numerous attempts have been reported to incorporate inorganic particles into PTMSP matrices to improve the mechanical resistance and selectivity in gas separations, but only Woo and Tsapatsis [15] used a zeolite, ZSM-5, to enhance PTMSP performance in butane isomers separation. Zeolites are porous crystalline alumino-silicates composed of $AlO_2$ and $SiO_2$ tetrahedra, and the Si/Al ratio can be varied in a wide range, and the incorporation of elements different from both aluminum and silicon is also possible. The adsorption capacity of zeolites is due to their regular and stable porous structure, composition of extra-frameworks cations and to the Si/Al ratio. This strongly influences in particular the uptake of $CO_2$ [18]. LTA-type zeolites have been shown to have good working capacities that can be modified according to the chosen process conditions [19].

A significant effort has been devoted to prepare membranes using zeolite A (LTA structure) as filler in rubbery polymers, such as polydimethyl siloxane (PDMS) [20, 21], or PEBAX [22], because the small molecular sieve size (0.4 nm) and shape selective properties help increasing the mechanical stability and selectivity of these polymers. The compatibility between the LTA filler and polymer can be controlled by tuning up the Si/Al ratio to enhance the adhesion between the phases. The addition of zeolite A in glassy polymers such polyethersulfone (PES) has also been largely studied [23], although in this case the MMM preparation involves complications such as the use of organic additives and priming in order to increase the adhesion between the zeolite and the polymer matrix [24]. Priming was not observed to have any influence on the membrane quality in the preparation of ITQ-29-polysulfone MMMs, as much as other conditions such solvent type and drying procedure [25].

In this work, small pore LTA zeolites with Si/Al ratio of 1 and ∞ (ITQ-29) were selected to improve the PTMSP separation performance in $CO_2/N_2$ separation. $CO_2$ and $N_2$ gas permeation performance was evaluated at different temperatures and zeolite loadings, taking into account the thermal and mechanical stability. Membranes were characterized by scanning electron microscopy, thermo gravimetric and differential thermal analyses, X-ray diffraction and permeation of $CO_2$ and $N_2$ and the transport properties were fitted to Maxwell-based models as a function of temperature and morphology.

## 2. Experimental

### 2.1 Membrane preparation

Polymer and mixed matrix membranes were prepared by the solution casting method. In a typical synthesis, poly(1-trimethylsilyl-1-propyne) (PTMSP, Gelest) was

dried at 333K to eliminate all humidity, before being dissolved in toluene to a 1.5 wt. % polymer solution, for 24 h at 333K. After that, the solution was filtered under vacuum to eliminate impurities. The selected volume was degassed in an ultrasound bath for 10 min before casting onto a glass plate. The films were allowed to dry slowly covered by a Petri dish at ambient conditions. Removal of the film from the glass substrate was carried out by washing with copious amounts of deionized water. Some membranes were measured as-made, and others were stored in liquid methanol and dried before gas permeation experiment, in order to prevent physical aging. At last, membrane immersion in methanol for 5 min before the gas permeation tests, was the method that prevailed to control physical aging and obtain reproducible permeation results.

For the MMMs, the procedure was similar. The zeolites were dried at 373K for several hours then dispersed in the solvent for 2h before adding the polymer solution. The nominal zeolite loading was varied in the range from 5 to 20 wt. % to PTMSP polymer ratio. The mixture was stirred for 24h before continuing the procedure as in the PTMSP membranes.

The zeolites used as fillers in this work were commercial zeolite A, with Si/Al = 1 (Molecular sieves 4A, Aldrich) and pure silica ITQ-29, prepared as reported in a previous work [25]. Both have an average particle size of 2.5 μm. The molecular structure of PTMSP and LTA framework are shown in Fig. 1.

The membrane thickness was carefully measured using a digital micrometer (Mitutoyo digimatic micrometer, IP 65) with a precision up to 0.001 mm. Five points of the membrane effective area were measured and the average thickness and standard deviations were calculated therefrom. The dry weight of the membranes was also measured before each set of experiments. The density of selected membrane samples of every composition was also measured after the whole set of permeation experiments, to

monitor changes in density and check the absence of physical aging and the structural integrity of the membrane.

### 2.2 Membrane characterization

The pure gas permeability was measured using the experimental set up in Fig. 2. It consists of a membrane module, connected, by means of a series of pneumatic controlled valves, to the feed and permeate sides. The membrane module is placed in a convection oven (Memmert, Germany). The permeation cell is composed by two parts pneumatically pressed each other on a Viton ring that seals the membrane. Basically, the membrane was placed in a stainless steel permeation cell leading to an effective area about 14.05 $cm^2$. Two transducers (Omega, UK) measured the pressure in the feed side and across the membrane during the whole experiment, in order to monitor the gas volume which goes through it.

Gas permeation tests were carried out in a temperature range of 298 – 363K, feeding the single gases at 2 – 3 bar and evacuating the permeate to generate the pressure difference across the membrane. Gas permeation was tested in the following order: $N_2$ and $CO_2$, evacuating both the feed and the permeate side before each measurement, and checking the air tightness of the system. The same protocol has been followed for pure polymer and mixed matrix membranes.

The gas permeation through dense polymeric membranes is described by the solution-diffusion model in three major steps: (i) adsorption of the gas onto the membrane surface, diffusion across the membrane thickness and desorption from the permeate side,

$$P = D \cdot S \tag{1}$$

The permeability represents the amount of molecules that cross the membrane and is described by Eq. (1), where *D* is de diffusion coefficient and *S* the solubility coefficient.

Diffusivity (*D*) is the measure of the amount of mobility of the molecules passing through the voids of the polymer. The solubility (*S*) is related to the number of dissolved molecules in the polymer. Thus the permeability is given by the product of the diffusion coefficient, a kinetic factor, and the solubility coefficient, a thermodynamic factor, both being influenced by temperature.

Applying a mass balance to the membrane material, the following equation is achieved, where $P_i$ is the permeability constant, $\delta$ is the membrane thickness, $p_{i,f}$ is the partial pressure of the gas *i* in the feed side and $p_{i,p}$ is the partial pressure of the gas *i* in the permeate side. The pure gas permeability was calculated from the feed and permeate pressures by Eq. (2) [26].

$$ln\left|\frac{\left(p_{i,f}-p_{i,p}\right)_0}{\left(p_{i,f}-p_{i,p}\right)}\right| = ln\left|\frac{\Delta p_0}{\Delta p}\right| = \left(\frac{P}{\delta}\right)\beta_m t \quad (2)$$

Where $\beta_m$ is a geometric factor depending from the feed and permeate volume compartments and the effective membrane area, with a value of 81.04 $m^{-1}$ for the experimental system used in this work. Thus, the permeability can be calculated from the slope of the linear representation of Eq. (2) once steady state is reached.

The ideal selectivity is the ability to separate two molecules of a mixture (e.g., $CO_2$ and $N_2$, in this work) thus it is an intrinsic property of the membrane material, which can be calculated from the ratio of the pure gas permeabilities, defined by Eq. (3).

$$\alpha = \frac{P_{CO_2}}{P_{N_2}} \quad (3)$$

Therefore, the difference between permeabilities of different gases through the membrane is not only due to the diffusivity, but also influenced by the physicochemical interactions of these gases with the membrane material, which determines the amount of gas flowing per unit volume (*S*). Membranes should present both high permeability and

selectivity, because a high permeability will make necessary a smaller membrane area, while a high selectivity provides a greater purity of gas at the exit.

Thermal resistance of the samples was studied by thermo gravimetric analyses (DTA-TGA). These analyses were performed using a thermo balance (DTG-60H, Shimadzu, Japan) in air at heating rate of 283K/min up to 973K Samples of approximately 2 – 5 mg were loaded into an alumina crucible and a reference pan was left empty during the experiment.

The crystalline structure of the samples was investigated by means of room temperature X-ray powder diffraction (XRD). The patterns were collected on a Philips X'Pert PRO MPD diffractometer operating at 45 kV and 40 mA, equipped with a germanium Johansson monochromator that provides Cu Kα1 radiation (λ = 1.5406 Å), and a PIXcel solid angle detector, at a step of 0.05º.

The morphology and cross-sectional areas of selected membranes were observed by scanning electron microscopy, using a JEOL JSM 5410 equipment, at the Universidad Politécnica de Valencia. Membrane samples were immersed in liquid nitrogen prior to being fractured and sputtered with gold before observation.

## 3. Results and discussion

Thermogravimetric analyses (TGA) of the membranes are presented in Fig. 3. In the case of the membranes, thermal degradation starts at 573K and kept small up to 623K. The shape of the curves is very similar to that of the pure polymer because of the low zeolite/polymer concentration ratio. In general, the real zeolite loading of the membranes agrees with nominal value and the thermal stability of the membranes is similar to the glassy polymer PTMSP. The real loading of the zeolite has been calculated from the TGA analyses as 7.06 ± 2.07 and 20.04 ± 1.36 wt. % for 5 and 20 wt. % Zeolite A-PTMSP

MMMs, respectively. In the case of ITQ-29-PTMSP MMMs, the real loading of zeolite is 11.8 ± 6.86 wt. % and 28.6 ± 8.84 wt. % for 5 and 20 wt. % ITQ-29 MMMs, respectively. This shows a greater dispersion of the pure silica ITQ-29 particles in the PTMSP matrix, than zeolite A. This also indicates that the MMMs are thermally stable up to 573K, which accounts for the potential of these membrane materials in high temperature separation processes.

The X-ray diffraction (XRD) patterns of the membranes are presented in Fig. 4. The characteristic reflections of zeolite A and ITQ-29 become stronger with increasing loading, thus revealing their presence into the polymer matrix. In general, the narrowness of a XRD peak with strong intensity indicates a crystalline nature and if the diffraction peak is broader than the polymer is amorphous in nature. The main peaks of high intensities in zeolite A are at around 7º, 10º, 24º, 27º of diffraction angle. PTMSP is an amorphous polymer but with increasing zeolite A loading, a slight shift of the broad band to higher angles is observed, derived from the interaction between zeolite and polymer occurring in the case of zeolite A, which does not occur in the case of ITQ-29, where there might be some changes in orientation because of the appearance of voids by the poor contact between the pure silica zeolite particles and the PTMSP polymer.

The interaction between the PTMSP and the zeolite particles depend on Si/Al ratio. The smaller ITQ-29-PTMSP than zeolite A-PTMSP interaction is further observed by SEM in Fig. 5d and 5e, where the good adhesion and dispersion at 5 wt. % ITQ-29 loading disappears when the zeolite loading is increased, leading to voids and defects. Examples are highlighted by circles. The differences in zeolite composition lead to an asymmetric morphology in both types of membranes. On one hand, in ITQ-29-PTMSP MMM, the zeolite particles with higher density (1.42 g/cm$^3$) than the polymer (0.75 g/cm$^3$) accumulate at the bottom of the membrane, even more than observed for ITQ-29-

polysulfone [25], because of the higher difference in densities when the polymer is PTMSP. The low adhesion and compatibility increases the number of voids and the performance of the MMM is deteriorated [27]. On the other hand, zeolite A particles also accumulate at higher loadings because of the difference of densities with PTMSP (1.27 $g/cm^3$ vs. 0.75 $g/cm^3$). In this case, two distinct layers appear, a top almost pure PTMSP layer and a bottom zeolite A layer where the PTMSP acts as binder. These membranes obtained values of $CO_2$ permeability and $CO_2/N_2$ selectivity as high as 20000 Barrer and 76, respectively, which proves the good adhesion/compatibility of the low Si/Al ratio zeolite filler with this polymer.

The $CO_2$ permeability values and $CO_2/N_2$ selectivities of the zeolite A-PTMSP and ITQ-29-PTMSP membranes are plotted in Fig. 6 as a function of temperature. The permeability of pristine PTMSP membranes decreases with temperature because of the high free volume, rigid and weakly molecular sieving structure is more prone to changes in solubility than diffusivity [30, 31]. The $CO_2$ permeability of MMMs also decreases with temperature, although reaching maximum values at a 20 wt. % zeolite A content. The selectivity of the MMMs is higher than that of pure PTMSP membranes, especially for zeolite A loadings, in the range of temperature under study. However, the selectivity of ITQ-29-PTMSP MMMs decreases from 5 to 20 wt. % zeolite loadings, because of the appearance of voids caused by lower interaction polymer-pure silica zeolite. For this reason, we believe that the zeolite particles introduce a molecular sieving effect leading to an increased selectivity at an optimal zeolite loading, which is also dependent on the interaction between the zeolite filler and the PTMSP matrix, and this on the Si/Al composition of the zeolite, and independent of temperature in the range studied in this work.

In the MMMs prepared in this work, the influence of temperature on permeability changes from 5 to 20 wt. % zeolite loading, as compared to the pure polymer membrane (Fig. 7). The activation energies for permeation are -7.1 ± 1.4 and -12.6 ± 4.1 kJ/mole, for $CO_2$ and $N_2$ through pure PTMSP membranes, respectively, in agreement with literature [31]. The activation energies for permeation through the MMMs are presented in Table 1. These values increase with zeolite A loading content, revealing there is a crosslinking interaction phenomenon occurring between the fillers and the PTMSP [13]. The activation energies for the permeation through ITQ-29-PTMSP MMMs increase largely in the case of 5 wt. % and decrease again at higher loadings. The ITQ-29 particles can indeed produce tortuosity and enhance selectivity only when the interaction and dispersion in the polymer matrix is good; for pure silica ITQ-29 this only occurs at low loadings [25].

In this work, it is the permselectivity that increases with temperature and zeolite loading. Fig. 8 allows comparison of the permselectivity of MMMs as a function of zeolite loading, against existing membrane materials, using the Robeson's upper bound. In the case of zeolite A-PTMSP MMMs, the $CO_2/N_2$ selectivity increases with filler concentration. The larger the zeolite A concentration, the better the permeability and the selectivity. The Robeson's upper bound is overcome for increasing zeolite A concentrations, despite the two-layer morphology [27]. This allows inferring a good adhesion between the low Si/Al ratio zeolite and the PTMSP, which does not occur for the pure silica ITQ-29-PTMSP MMMs, where the permselectivity of pure PTMSP membranes is only surpassed at the lowest zeolite loading, 5 wt. %, as in other glassy polymer-based MMMs, where poor interfacial contact enhances the appearance of voids with increasing zeolite loading, thereby deteriorating selectivity [28]. The differences found between zeolite A and ITQ-29-based MMMs are attributed here to the different

Si/Al ratio, which may affect the interaction with the solvent and the polymer chains upon mixing, and thus the performance of the MMMs [29].

MMM performance can be adjusted to various theoretical expressions as a function of membrane morphology imposed by filler loading [20]. The minimum value of effective permeability occurs when considering a series mechanism of transport through the two phases and expressed as Eq. (4). $P_c$ is the permeability through the continuous PTMSP matrix, based on experimental values, and $P_d$, the permeability of the gas through the dispersed zeolite filler which, for this work, is taken from Shen and Lua [32] for zeolite A membranes, and [33] for the ITQ-29 membrane.

$$P_{eff} = \frac{P_c P_d}{\phi_c P_d + \phi_d P_c} \tag{4}$$

The maximum value of the effective permeability is taken when both phases are assumed to work in parallel to the flow direction, as in Eq. (5)

$$P_{eff} = P_c \phi_d + P_d \phi_c \tag{5}$$

Maxwell equation, is still the most widely accepted to interpret the transport properties of MMMs [20]. The theoretical calculation of the overall steady-state composite permeability is given by Eq. (6).

$$P_{eff} = P_c \left( \frac{P_d + 2P_c - 2\phi_d \left( P_c - P_d \right)}{P_d + 2P_c + \phi_d \left( P_c - P_d \right)} \right) \tag{6}$$

These theoretical permeabilities are plotted against experimental permeabilities in Fig. 9 as a function of zeolite loading and temperature. The behavior varies with Si/Al ratio as commented above. For the zeolite A-PTMSP MMMs, the experimental values are between parallel and series models and Maxwell overestimates $N_2$ permeability while adjusting $CO_2$ permeability at low loading. At high loadings, the Zeolite A-PTMSP MMM performance cannot be fitted to these models because of the asymmetric

morphology, closeness between the particles and the polymer, and good interaction between the low Si/Al ratio and the PTMSP polymer. For the pure silica ITQ-29-MMM, a “sieve-in-a-cage” morphology can be diagnosed at higher loadings where the experimental permeability is always higher than the calculated values, because poor interaction between ITQ-29 and the polymer [20], leading to interfacial voids or defects between the polymer and the particle as those discerned by SEM. When the zeolite was well dispersed in the matrix, at 5 wt. % loading, the Maxwell model overestimates gas permeability and this can be attributed to discrepancies between literature diffusion and solubility values used in model predictions [20].

In order to account for interfacial defects affecting membrane performance, the two-phase modified Maxwell model was applied to adjust the permeability of a pseudo-interphase induced by those interfacial voids [29]. The calculated permeability values are compared with experimental ones as a function of temperature and zeolite loading and Si/Al ratio in Fig. 10. These equations are based on two parameters that can be estimated in an iterative way to adjust the experimental and calculated permeabilities with an experimental error up to 10%: the thickness of the interphase between the polymer and the zeolite, $l_I$ (μm), accounting for the possible presence of voids and defects leading to increased permeability and reduced selectivity and the chain immobilization factor, $\beta$, accounting for the polymer matrix rigidification, leading to increased selectivity and reduced permeability. The parameter $\beta$ depends upon the nature of the gas molecule, since it has different values for $CO_2$ and $N_2$ [34] and decreases with operation temperature, as summarized in Tables 2 and 3 for Zeolite A and ITQ-29-PTMSP MMMs. The parameter $l_I$ (μm) is influenced by the Si/Al ratio of the zeolite fillers, [27] which we attribute to the different interaction with the polymer matrix and membrane performance varying with temperature. The interphase thickness in low Si/Al zeolite MMMs was independent of

the type of gas and temperature, while for the pure silica ITQ-29 MMMs, parameter $l_I$ was also independent of zeolite loading, because of the poor adhesion leading to voids that decrease selectivity for the 20 wt. % ITQ-29-PTMSP membrane.

The modelling results shown in Fig. 10 indicates that influence of temperature on the permeability of pure silica ITQ-29-PTMSP membranes can be taken into account by the assumptions of modified Maxwell model if the membrane does not have defects. The performance of zeolite A-PTMSP MMMs deviates from the modified Maxwell model of the zeolite A-PTMSP MMMs performance at high loadings because of the asymmetric morphology and the good interaction of low Si/Al LTA-type zeolite with the glassy PTMSP polymer. This phenomenon leads to an increase in $CO_2$ permeability and a decrease in $N_2$ flux as in a pure zeolite membrane [35]. This effect is even more remarkable with increasing temperature because of the higher $CO_2$ permselectivity of zeolite A- than ITQ-29-PTMSP MMMs with increasing temperature and zeolite loading.

## 4. Conclusions

Mixed Matrix Membranes (MMMs) were prepared using highly permeable PTMSP polymer and small pore LTA-type zeolites with Si/Al ratio of 1 and ∞ (ITQ-29) by the solution-casting method. Both zeolites maintained the thermal stability of the PTMSP in the MMMs. The permselectivity of $CO_2$ and $N_2$ increased with the increase in zeolite loading, much more enhanced for $CO_2$ than $N_2$. This is attributed to the appearance of molecular sieving effect upon zeolite introduction, which was maintained even when increasing the temperature. The membranes prepared with low Si/Al ratio zeolite A showed the highest $CO_2$ permeability and selectivity, even surpassing the Robeson's upper bound. The performance of LTA-type zeolite-PTMSP MMMs can be adjusted to the modified Maxwell model if Si/Al, temperature and morphology are considered, not

only the zeolite loading. However, the permeability of zeolite A-PTMSP MMMs at high loadings is much higher than those predicted by the known models, because of the asymmetric morphology and good adhesion. These results highlight the importance of the compatibility of fillers and polymers in mixed matrix membrane technology and the potential of these kind of membranes in high temperature $CO_2$ separation.

## 5. Acknowledgements

Financial support from the Spanish Ministry of Economy and Competitiveness (MINECO) under project CTQ2012-31229 at the Universidad de Cantabria is gratefully acknowledged. A.F.B. and C.C.C. also thank the MINECO for the Early Stage Researcher (BES2013-064266) and "Ramón y Cajal" (RYC2011-0855) grants, respectively. M.P. and S.V. also thank the financial support from the Spanish Government (MAT2012-38567-C02-01, Consolider Ingenio 2010-Multicat CSD-2009-00050 and Severo Ochoa SEV-2012-0267).

## 6. Symbols used

*Symbols*

| | | |
|---|---|---|
| $D$ | [$m^2\ s^{-1}$] | diffusivity coefficient |
| $p$ | [bar] | partial pressure |
| $S$ | [$cm^3\ cm^{-3}\ cmHg^{-1}$] | solubility coefficient |
| $P$ | [Barrer] | permeability (1 Barrer= $7.5005 \cdot 10^{-18} m^2 s^{-1}\ Pa^{-1}$) |
| $l_i$ | [μm] | Interphase thickness |

*Greek letters*

| | | |
|---|---|---|
| $\delta$ | [m] | thickness |
| $\theta$ | [s] | time lag |
| $\beta_m$ | $m^{-1}$ | geometric factor |
| $\alpha$ | [–] | ideal selectivity |
| $\phi$ | [–] | volume fraction |
| $\beta$ | [–] | Chain rigidification factor |

*Subscripts*

| | |
|---|---|
| f | feed side |
| p | permeate side |
| eff | effective |
| d | dispersed phase |
| c | continuous phase |

## 7. References


[1] R. S. Haszeldine, *Science* **2009**, *325*, 1647.

[2] A. Del Castillo, M. Alvarez-Guerra, A. Irabien, *AIChE J.* **2014**, *60*, 3557.

[3] B. T. Low, L. Zhao, T. C. Merkel, M. Weber, D. Stolten, *J. Membr. Sci.* **2013**, *431*, 139.

[4] C. Casado-Coterillo, T. Yokoo, T. Yoshioka, T. Tsuru, M. Asaeda, *Sep. Sci. Technol.* **2011**, *46*, 1224.

[5] R. Bredesen, K. Jordal, O. Bolland, *Chem. Eng. Proc.* **2004**, *43*, 1129.

[6] J. Gascón, F. Kapteijn, B. Zornoza, V. Sebastián, C. Casado, J. Coronas, *Chem. Mater.* **2012**, *24*, 2829.

[7] A. Lee, G. Xiao, P. Xiao, K. Joshi, R. Singh, P. A. Webley, *Energy Proc.* **2011**, *4*, 1199.

[8] L. M. Robeson, *J. Membr. Sci.* **2008**, *320*, 390.

[9] C. E. Powell, G. G. Qiao, *J. Membr. Sci.* **2006**, *279*, 1.

[10] S. Matteucci, V. A. Kusuma, D. Sanders, S. Swinnea, B. D. Freeman, *J. Membr. Sci.* **2008**, *307*, 196.

[11] K. Nagai, T. Masuda, T. Nakagawa, B. D. Freeman, I. Pinnau, *Prog. Pol. Sci.* **2001**, *26*, 721.

[12] A. Morisato, H. C. Shen, S. S. Sankar, B. D. Freeman, I. Pinnau, C. G. Casillas, *J. Polym. Sci. B* **1998**, *34*, 2209.

[13] J. Qiu, K.-V. Peinemann, *Desal.* **2006**, *199*, 113.

[14] C. H. Lau, P. T. Nguyen, M. R. Hill, A. W. Thornton, K. Konstas, C. M. Doherty, R. J. Mulder, L. Bourgeois, A. C. Y. Liu, D. J. Sprouster, J. P. Sullivan, T. J. Bastow, A. J. Hill, D. L. Gin, R. D. Noble, *Angew. Chem. Int. Ed.* **2014**, *53*, 5322.

[15] M. Woo, J. Choi, M. Tsapatsis, *Micropor. Mesopor. Mat.* **2008**, *110*, 330.

[16] T.-S. Chung, L. Y. Jiang, Y. Li, S. Kulprathipanja, *Prog. Pol. Sci.* **2007**, *32*, 483.

[17] R. Mahajan, R. Burns, M. Schaeffer, W. J. Koros, *J. Appl. Pol. Sci.* **2002**, *86*, 881.

[18] D. Bonenfant, M. Kharoune, P. Niquette, M. Mimeault, R. Hausler, *Sci. Technol. Adv. Mater.* **2008**, *9*, 013007 (7pp).

[19] M. Palomino, A. Corma, F. Rey, S. Valencia, *Langmuir* **2009**, *26*, 1910.

[20] G. Clarizia, C. Algieri, E.Drioli, *Polymer* **2004**, *45*, 5671.

[21] M. Hussain, A. König, *Chem. Eng. Technol.* **2012**, *35*, 561.

[22] R. R. Murali, A. F. Ismail, M. A. Rahman, S. Sridhar, *Sep. Purif. Technol.* **2014**, *129*, 1.

[23] Y. Li, W. B. Krantz, T.-S. Chung, *AIChE J.* **2007**, *53*, 2470.

[24] R. Nasir, H. Mukhtar, Z. Man, D. F. Mohshim, *Chem. Eng. Technol.* **2013**, *36 (5)*, 717.

[25] C. Casado-Coterillo, J. Soto, M. T. Jimaré, S. Valencia, A. Corma, C. Téllez, J. Coronas, *Chem. Eng. Sci*. **2012**, *73*, 116.

[26] E. L. Cussler, *Diffusion. Mass transfer in fluid systems*, 3rd ed., Cambridge University Press, Cambridge, **2007**.

[27] C. I. Chaidou, G. Pantoleontos, D. E. Koutsonikolas, S. P. Kaldis, G. P. Sakellaropoulos, *Sep. Sci. Technol.* **2012**, *47*, 950.

[28] Y. Cheng, R. H. Liao, J. S. Li, X. Y. Sun, L. J. Wang, *J. Mater. Proc. Technol.* **2008**, *206*, 445.

[29] T. T. Moore, R. Mahajan, D. Q. Vu, W. J. Koros, *AIChE J.* **2004**, *50*, 311.

[30] B. W. Rowe, B. D. Freeman, D. R. Paul, *Polymer* **2009**, 50, 5565-5575.

[31] T. C. Merkel, R.P. Gupta, B .S. Turk, B.D. Freeman, *J. Membr. Sci.* **2001**, *191*, 86.

[32] Y. Shen, A. C. Lua, *AIChE J.* **2013**, *59*, 4715.

[33] A. Huang, J. Caro, *Chem. Comm.* **2010**, *46*, 7748.

[34] Y. Li, H.-M. Guan, T.-S. Chung, S. Kulprathipanja, *J. Membr. Sci.* **2006**, *275*, 17.

[35] V. Sebastián, I. Kumakiri, R. Bredesen, M. Menéndez, *J. Membr. Sci.* **2007**, *292*, 92.

[36] L. A. El-Azzami, E. A. Grulke, *Ind. Eng. Chem. Res.* **2009**, *48*, 894.

[37] P. Jha, J. D. Way, *J. Membr. Sci.* **2008**, *324*, 151.

[38] S. Husain, W. J. Koros, *J. Membr. Sci.* **2007**, *288*, 195.

**Tables**

**Table 1.** Activation energies for permeation for MMMs (kJ/mole).

| **Nominal zeolite loading [wt. %]** | **Zeolite A-PTMSP MMMs** | | **ITQ-29-PTMSP MMMs** | |
|---|---|---|---|---|
| | **$CO_2$** | **$N_2$** | **$CO_2$** | **$N_2$** |
| 5 | -3.25 ± 1.4 | -4.41 ± 2.0 | 35.90 ± 7.6 | 16.08 ± 1.5 |
| 20 | 17.21 ± 7.9 | 19.96 ± 10.7 | 15.19 | 3.01 |

**Table 2.** Modified model parameters estimated for adjusting the behavior of Zeolite A-PTMSP MMMs within 10 % experimental error.

| **T(K)** | **5 wt.% Zeolite A (Si/Al = 1)** | | | **20 wt.% Zeolite A (Si/Al = 1)** | | |
|---|---|---|---|---|---|---|
| | **$l_i$(μm)** | **β($CO_2$)** | **β($CO_2$)** | **$l_i$(μm)** | **β($CO_2$)** | **β($CO_2$)** |
| 298 | 4.95 | 1.2 | 55 | 2 | 1.2 | 14.8 |
| 303 | 2.7 | 0.85 | 18 | 0.95 | 0.59 | 6.6 |
| 313 | 2.87 | 0.86 | 7.6 | 1.1 | 0.53 | 3.63 |
| 323 | 2.6 | 0.28 | 9 | 1.1 | 0.14 | 0.94 |
| 333 | 2.5 | 0.27 | 15 | 1.1 | 0.13 | 0.7 |

**Table 3.** Modified model parameters estimated for adjusting the behavior of ITQ-29-PTMSP MMMs within 10 % experimental error.

| | 5 wt. % ITQ-29 (Si/Al = ∞) | | | 20 wt.% ITQ-29 (Si/Al = ∞) | | |
|---|---|---|---|---|---|---|
| **T(K)** | $l_i$**(μm)** | $\beta(CO_2)$ | $\beta(CO_2)$ | $l_i$**(μm)** | $\beta(CO_2)$ | $\beta$**(CO2)** |
| 298 | 1.8 | 4.1 | 18 | 0.8 | 0.36 | 0.47 |
| 303 | 1.8 | 2.7 | 15 | 0.8 | 0.23 | 0.51 |
| 313 | 1.8 | 2.05 | 12.3 | 0.8 | 0.165 | 0.43 |
| 323 | 1.8 | 0.315 | 2.4 | 1.2 | 0.175 | 0.22 |
| 333 | 1.8 | 0.21 | 1.75 | 1.2 | 0.17 | 0.186 |

**List of Captions**

**Figure 1.** Structure of PTMSP polymer (a) and LTA framework (b) of the zeolites used in this work.

**Figure 2.** Experimental setup for gas permeation measurements.

**Figure 3.** Thermal gravimetric analyses of zeolite A-PTMSP (a) and ITQ-29-PTMSP (b) MMMs.

**Figure 4.** X-ray diffractograms of the zeolite A-PTMSP (a) and ITQ-29-PTMSP (b) MMMs.

**Figure 5.** Cross-sectional morphologies of the MMMs: (a) pure PTMSP membrane, (b) 5 wt.% zeolite A-PTMSP, (c) 20 wt.% zeolite A-PTMSP, (d) 5 wt.% ITQ-29-PTMSP, and (e) 20 wt.% ITQ-29-PTMSP. Rule is 40 μm for Fig. 5a, 5b and 5c and 30 μm for Fig. 5d and 5d.

**Figure 6.** Effect of temperature on $CO_2$ permeability (a) and $CO_2/N_2$ selectivity of the zeolite A-PTMSP (▲) and ITQ-29-PTMSP (♦) MMMs at 5 wt. % (half-filled symbols) and 20 wt. % (full symbols). Pure dense PTMSP membrane's permeability and selectivity are also shown for comparison (○).

**Figure 7.** Arrhenius plots of the $CO_2$ permeability vs. temperature for zeolite A-PTMSP (a) and ITQ-29-PTMSP (b) MMMs, as a function of zeolite loading: 0 wt. % (■), 5 wt. % (♦) and 20 wt. % (▼).

**Figure 8.** Robeson's upper bound for $CO_2/N_2$ separation including the transport properties obtained experimentally at 298K for the PTMSP-based MMMs. Literature values for highly permeable polymers PTMSP [31], chitosan [36], PEBAX [18], PPZ [37], PDMS [38], are also included for comparison.

**Figure 9.** Comparison of series (dashed lines), parallel (dotted lines) and Maxwell (continuous lines) models with $CO_2$ (■) and $N_2$ (●) permeability experimental values for

Zeolite A-PTMSP (a) and ITQ-29-PTMSP (b) MMMs as a function of zeolite loading (5 wt. %: void symbols, 20 wt. %: full symbols) and temperature.

**Figure 10.** Comparison of modified Maxwell model prediction with experimental values of $CO_2$ (black squares) ■ and continuous lines for 20 wt. %, □ and dashed lines for 5 wt. % zeolite loading) and $N_2$ (grey circles) for Zeolite A-PTMSP (a) and ITQ-29-PTMSP (b) MMMs as a function of zeolite loading (5wt. %: void symbols and dashed lines, and 20 wt. %: full symbols and continuous lines).

**Figure 1.**

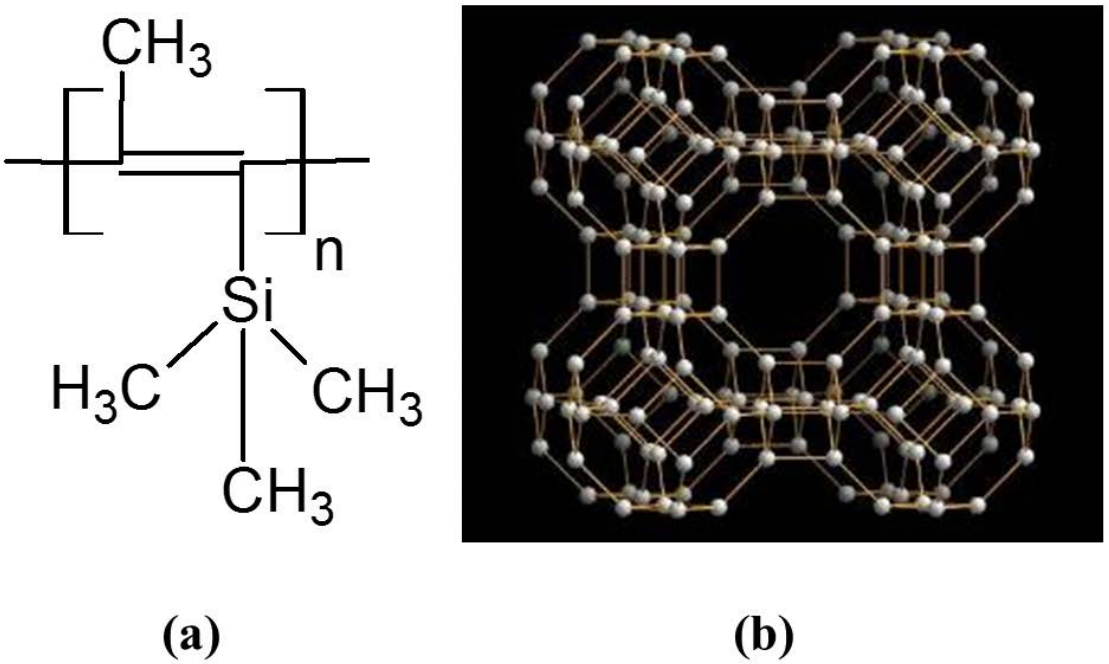


**(a)** **(b)**

**Figure 2**

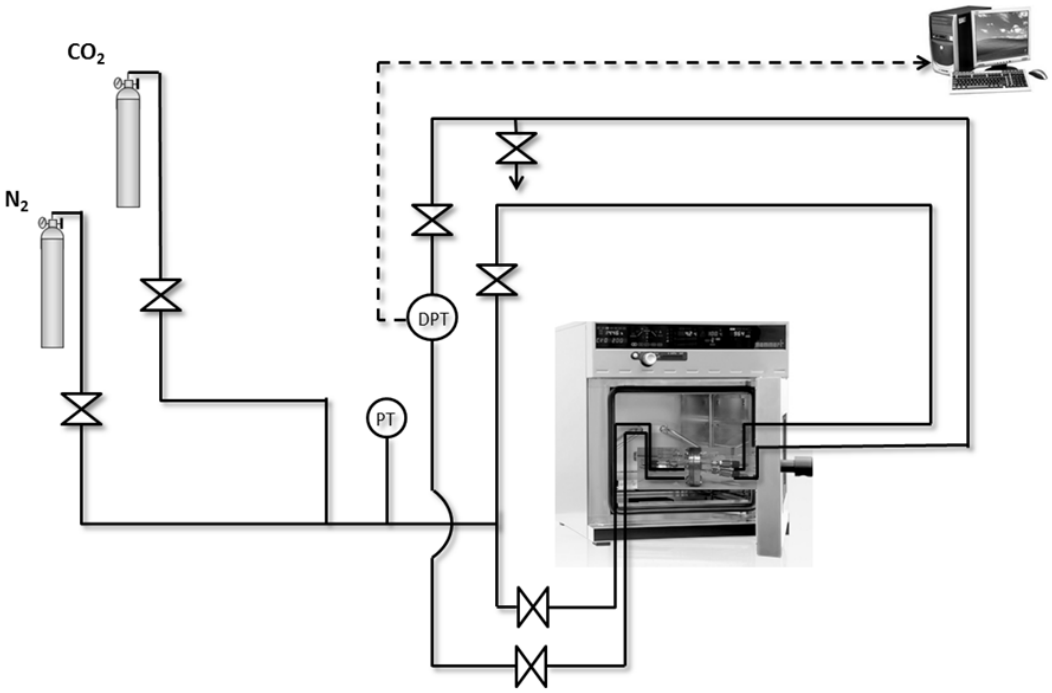

**Figure 3.**

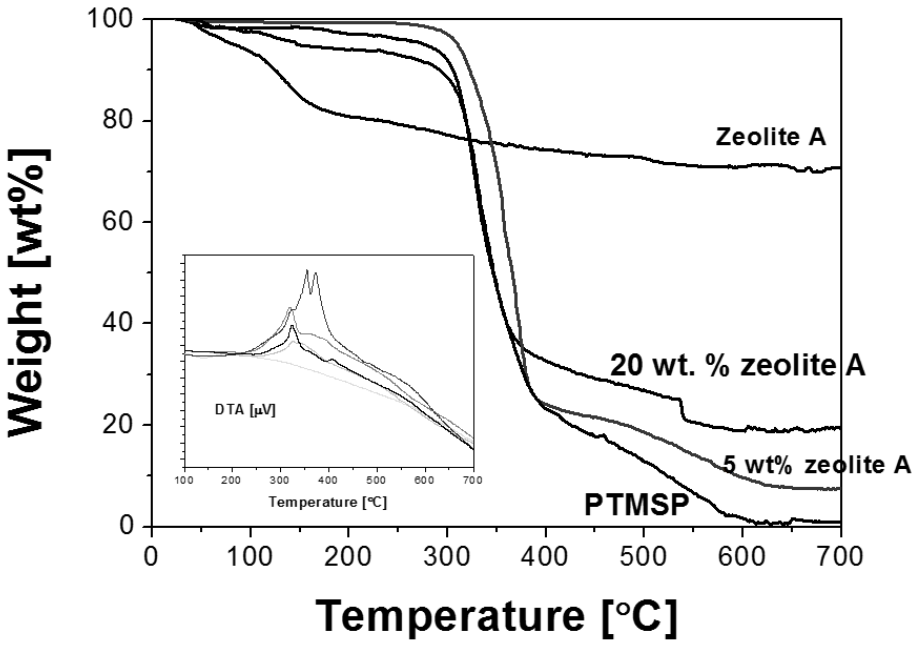
Weight [wt%]
Temperature [°C]
Zeolite A
20 wt. % zeolite A
5 wt% zeolite A
PTMSP
DTA [µV]
Temperature [°C]

**(a)**

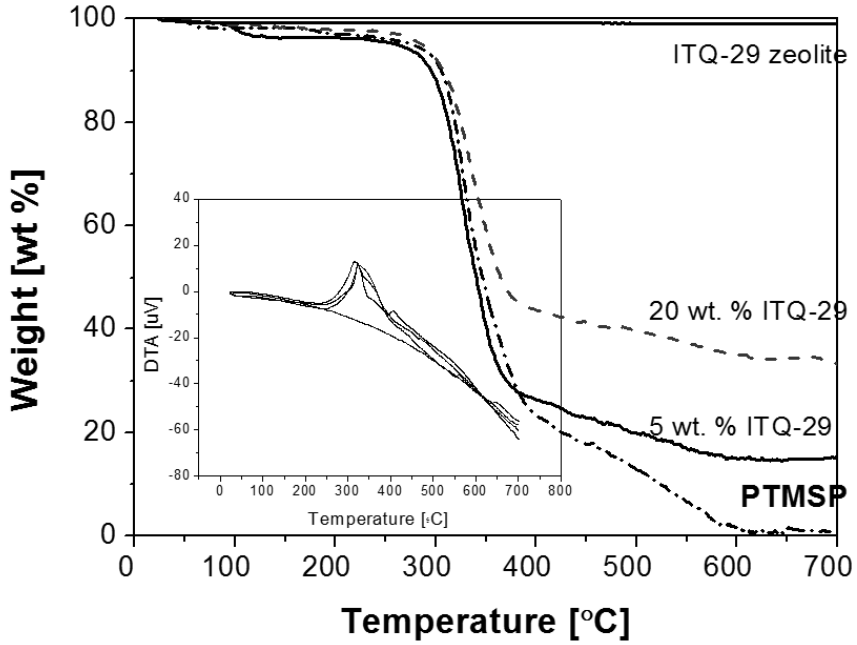
Weight [wt %]
Temperature [°C]
ITQ-29 zeolite
20 wt. % ITQ-29
5 wt. % ITQ-29
PTMSP
DTA [uV]
Temperature [°C]

**(b)**

**Figure 4**

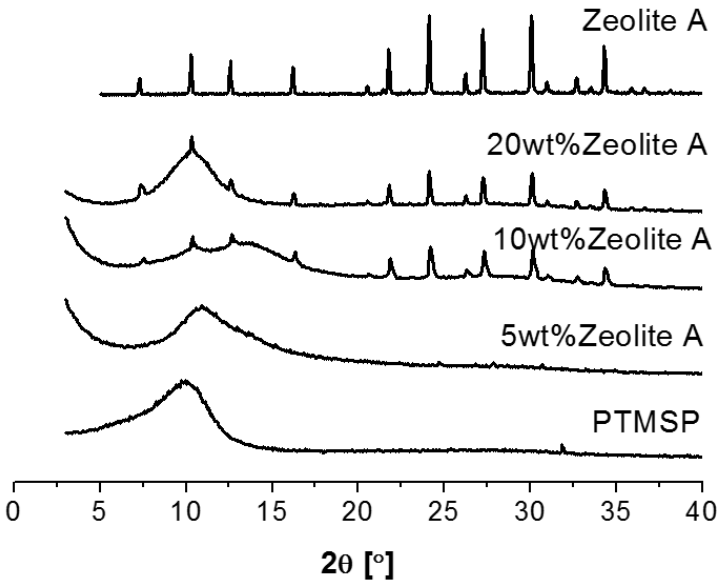
Zeolite A
20wt%Zeolite A
10wt%Zeolite A
5wt%Zeolite A
PTMSP
0
5
10
15
20
25
30
35
40
2θ [°]

**(a)**

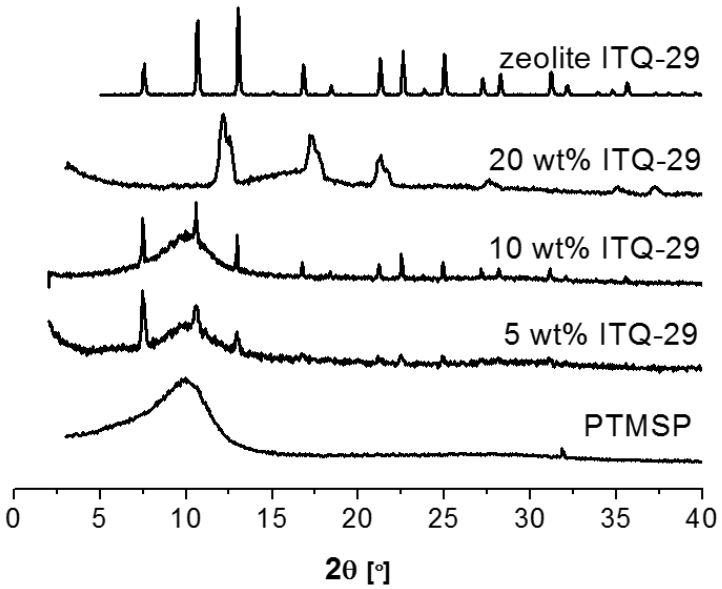
zeolite ITQ-29
20 wt% ITQ-29
10 wt% ITQ-29
5 wt% ITQ-29
PTMSP
0
5
10
15
20
25
30
35
40
2θ [°]

**(b)**

**Figure 5**

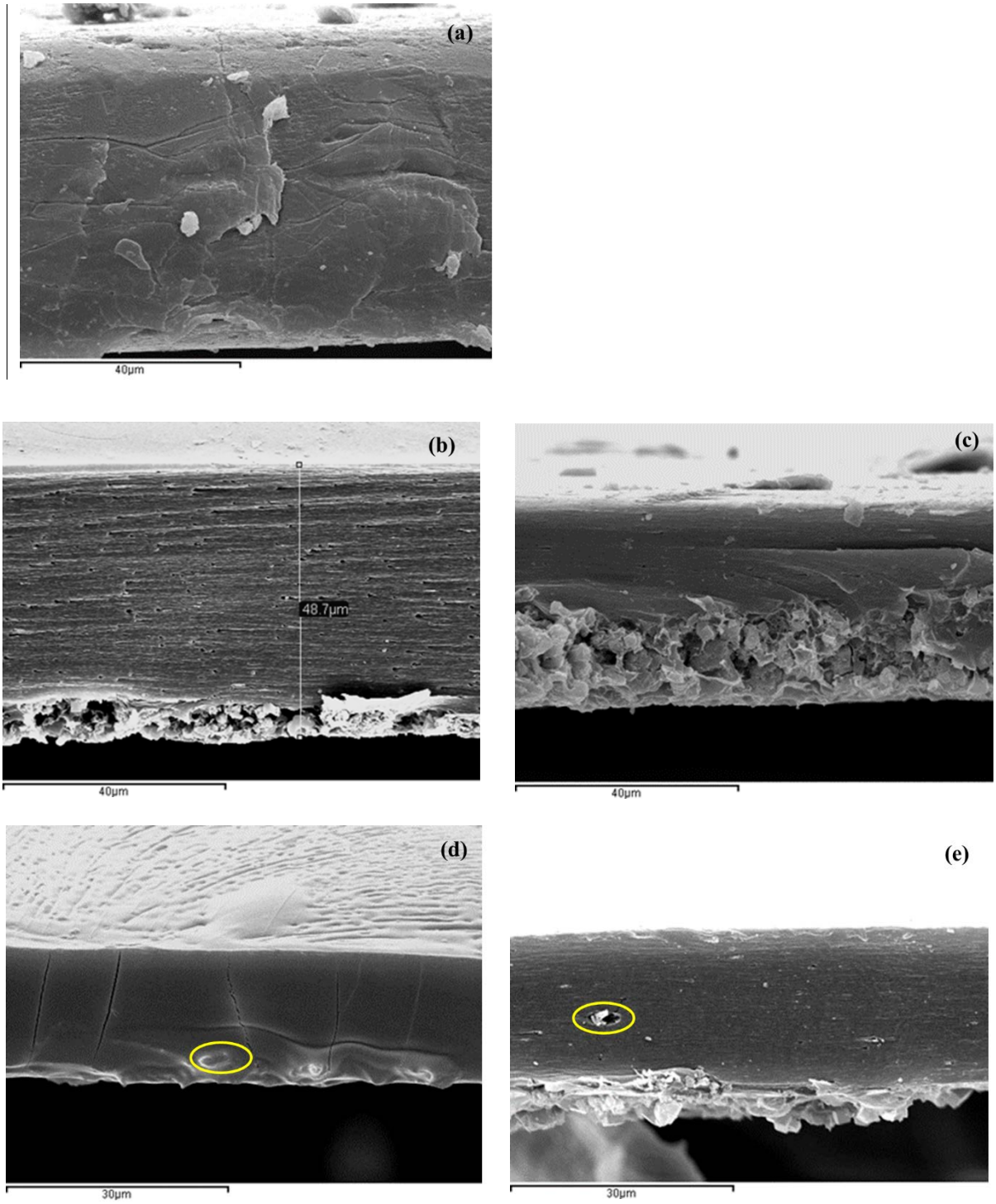

**Figure 6.**

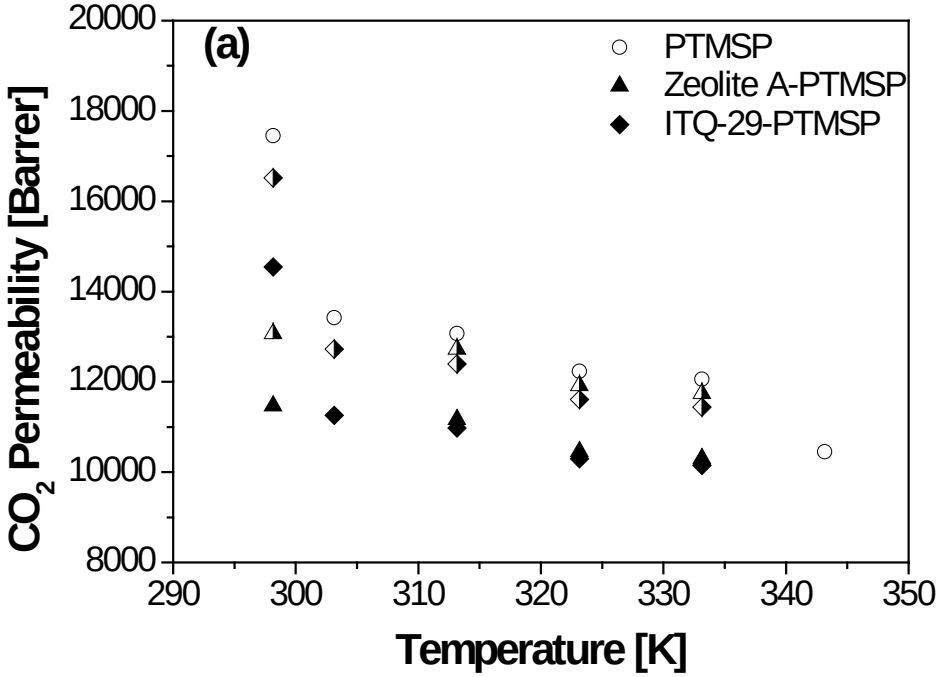
(a)
PTMSP
Zeolite A-PTMSP
ITQ-29-PTMSP
$CO_2$ Permeability [Barrer]
Temperature [K]
20000
18000
16000
14000
12000
10000
8000
290
300
310
320
330
340
350

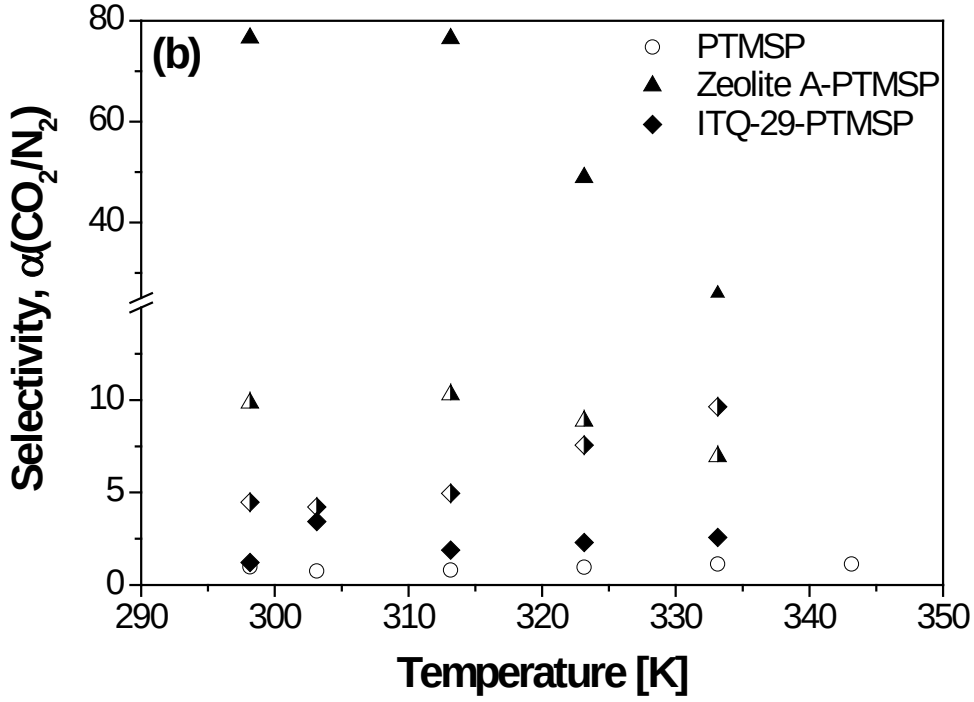
(b)
PTMSP
Zeolite A-PTMSP
ITQ-29-PTMSP
Selectivity, $\alpha(CO_2/N_2)$
Temperature [K]
80
60
40
10
5
0
290
300
310
320
330
340
350

**Figure 7.**

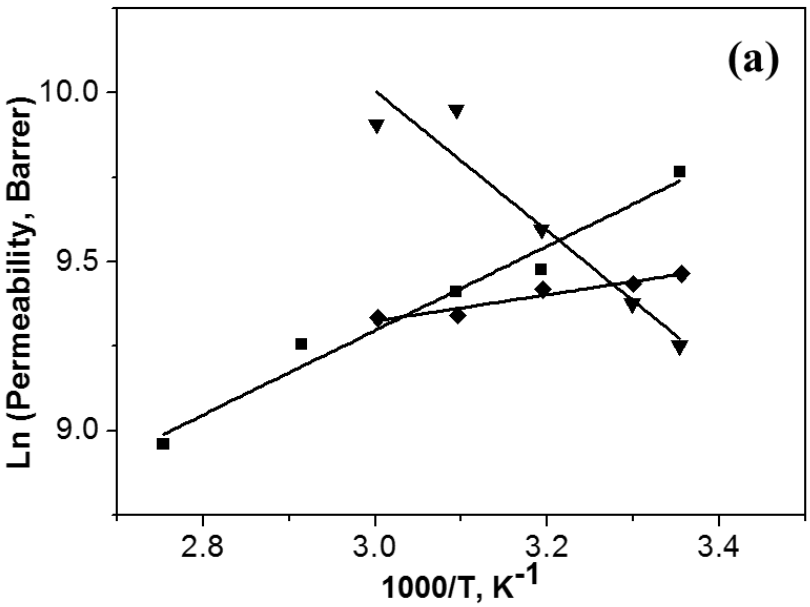
(a)
Ln (Permeability, Barrer)
10.0
9.5
9.0
2.8
3.0
3.2
3.4
1000/T, K-1

**(a)**

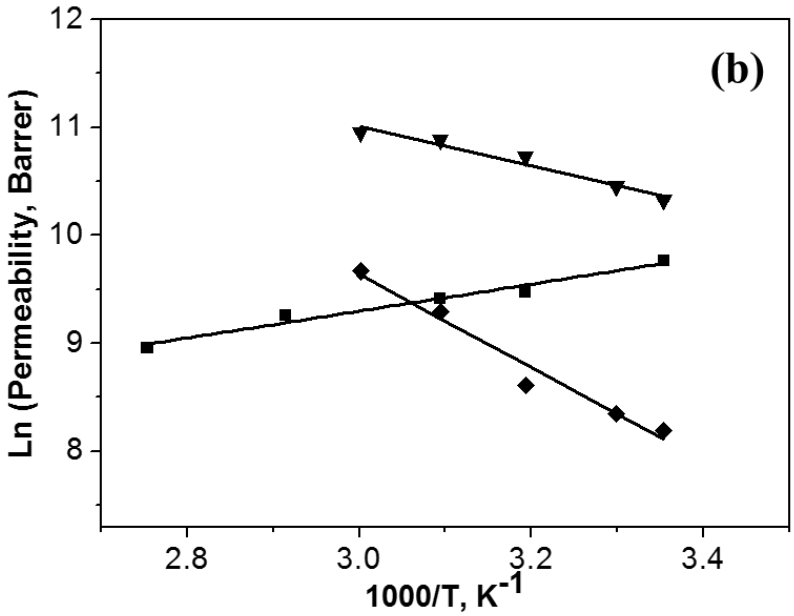
(b)
Ln (Permeability, Barrer)
12
11
10
9
8
2.8
3.0
3.2
3.4
1000/T, K-1

**(b)**

**Figure 8.**

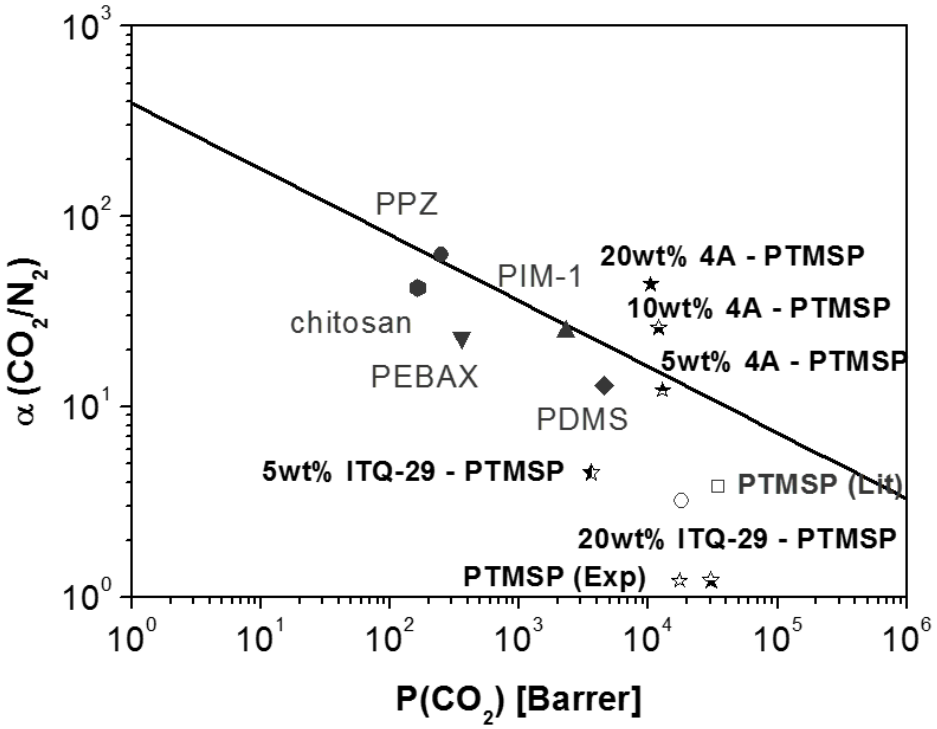
PPZ
PIM-1
chitosan
PEBAX
PDMS
20wt% 4A - PTMSP
10wt% 4A - PTMSP
5wt% 4A - PTMSP
5wt% ITQ-29 - PTMSP
PTMSP (Lit)
20wt% ITQ-29 - PTMSP
PTMSP (Exp)
α (CO2/N2)
P(CO2) [Barrer]

**Figure 9**

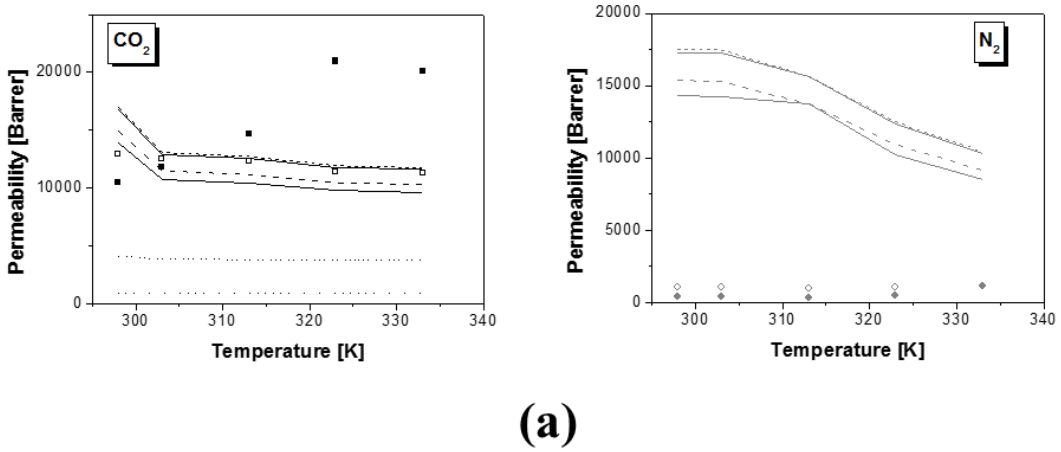
CO2
Permeability [Barrer]
Temperature [K]
N2
Permeability [Barrer]
Temperature [K]

**(a)**

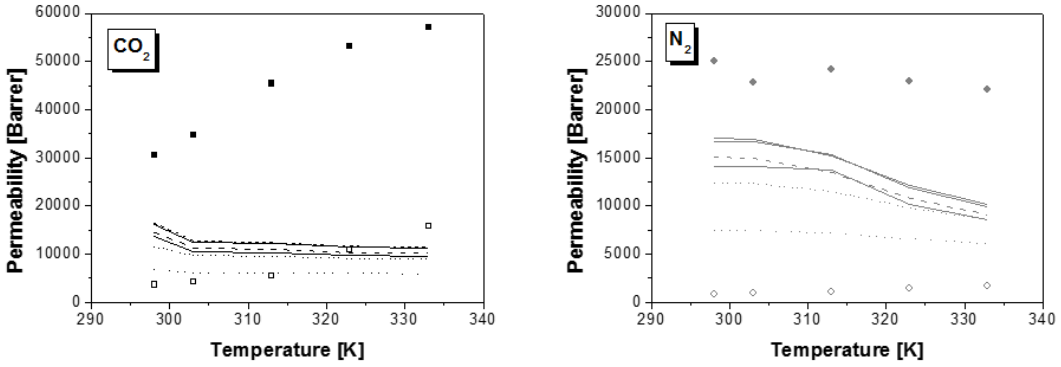
CO2
Permeability [Barrer]
Temperature [K]
N2
Permeability [Barrer]
Temperature [K]

**(b)**

**Figure 10**

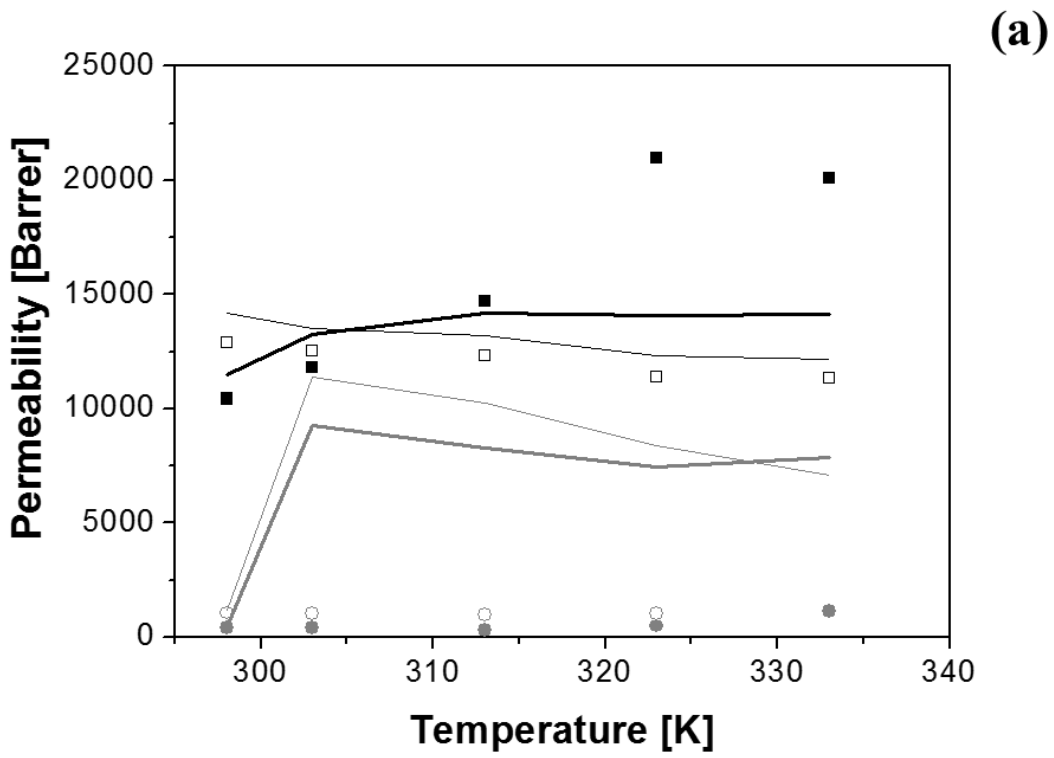
(a)
Permeability [Barrer]
25000
20000
15000
10000
5000
0
300
310
320
330
340
Temperature [K]

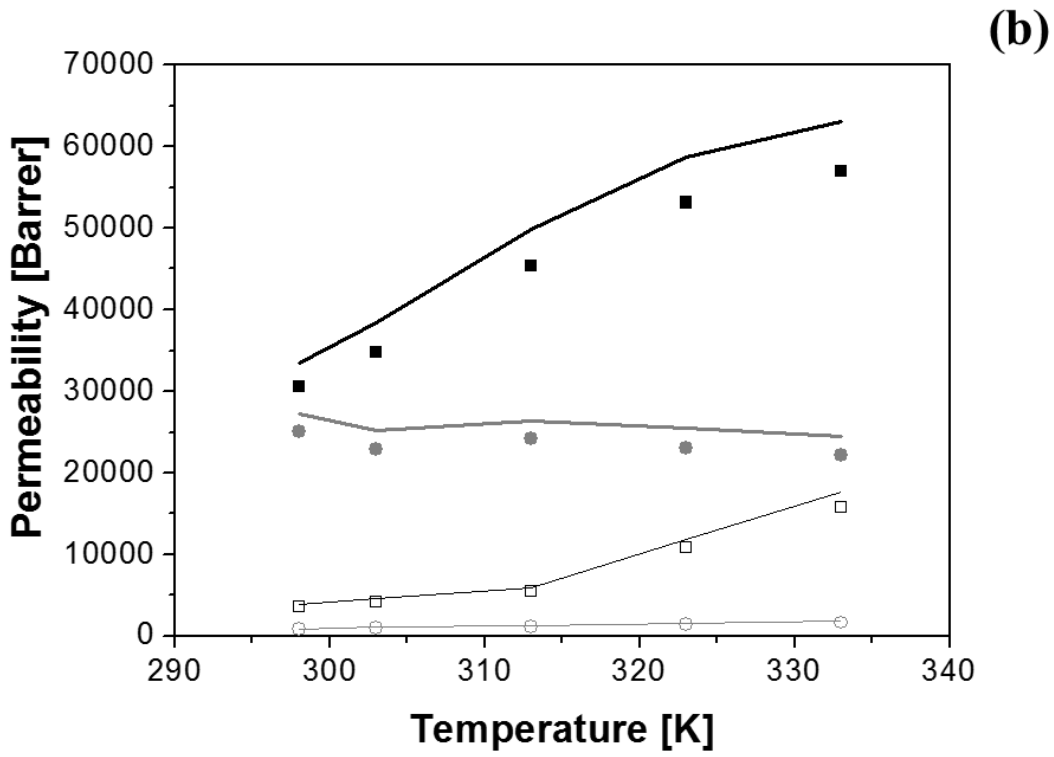
(b)
Permeability [Barrer]
70000
60000
50000
40000
30000
20000
10000
0
290
300
310
320
330
340
Temperature [K]